Enhancement of Reinforced Concrete Beam Capacity by Adding Cold-Formed Steel as Tensile Reinforcement

Indriyani Puluhulawa [1], Alamsyah [2*], Efan Tifani[3], Vina Runandhani [4]

{hf210022@student.uthm.edu.my[1], hf210014@student.uthm.edu.my[2], efantifani@polbeng.ac.id[3], vinarunandani@gmail.com[4] }

Universiti Tun Hussein Onn Malaysia [1,2] , State Polytechnic of Bengkalis [3,4]

Abstract. The utilization of cold-formed steel (CFS) as additional tensile reinforcement in coastal structure elements prone to higher corrosion risks presents the central concept of this research. It is widely recognized that CFS is equipped with a corrosion-resistant layer (zinc alloy) and boasts a higher yield strength compared to conventional bar reinforcement. Furthermore, by incorporating CFS as a composite material within reinforced concrete beams, the aim is to enhance flexural capacity without necessitating an increase in beam dimensions. Four reinforced concrete beams were constructed, with two serving as control beams and the other two incorporating CFS in varying cross-sectional configurations. The methodology involved experimental testing in a laboratory setting, with results subsequently compared to theoretical analyses. The findings of this study reveal that the addition of CFS as tensile reinforcement effectively elevates flexural capacity and augments beam stiffness.

Keywords: hybrid beam, cold-formed steel (CFS), flexural capacity

1 Introduction

The construction industry is rapidly advancing, particularly in the utilization of building materials such as concrete and steel. Furthermore, construction experts continuously conduct research to develop rapid and safe construction methods and techniques to address damages in building structures.

Reinforced concrete beams find extensive use in coastal structures, serving as building beams, wharves, and girders in bridges. The main constituent material is concrete, which is combined with reinforcing steel, commonly referred to as reinforced concrete. The inclusion of reinforcement in reinforced concrete beams aims to provide flexural resistance (tensile bars) and to withstand shear forces (stirrup).

In coastal marine construction, a frequent issue arises due to the rapid corrosion of the reinforcing steel within concrete, caused by the presence of seawater vapor containing Sodium

Chloride (NaCl). [1] points out that seawater significantly impacts concrete and structures. Structures located near the sea, such as those in Indonesia, are prone to exposure to sea salt, leading to a reduced lifespan of buildings. [2] revealed that seawater can decrease the shear strength of reinforced concrete beams by 10.7% compared to beams exposed to fresh water. This occurs due to the aggressive nature of seawater, leading to the formation of microcracks within concrete pores. These microcracks have the potential to trigger corrosion in the reinforcing steel, as highlighted by [3]. Ultimately, corrosion of steel reinforcement can result in the loss of serviceability or strength failure of reinforced concrete (RC) structures. To address the issue of corrosion, one strategy involves incorporating Fiber-Reinforced Polymer (FRP) into concrete. FRP, a non-corrosive fiber with high tensile strength, is known [4–8]. However, this high tensile strength can lead to brittle failure in reinforced concrete. Therefore, the design of FRP-reinforced concrete must consider compressive failure in the concrete.

Cold-formed steel (CFS) is another material with high tensile strength and non-corrosive properties. CFS is lighter compared to conventional steel due to its thin cross-section. With the advancement of the construction industry, CFS finds application in both secondary and primary structures [9]. Various tests have been conducted on CFS and concrete composites [10–14]. The research presented here combines CFS and reinforcing steel as flexural reinforcement in hybrid beams. The aim is to study the behavior of CFS hybrid beams, ascertain the extent of increased flexural capacity in these beams, and evaluate the influence of different CFS cross-sectional profiles on hybrid beams.

Figure 1 provides stress-strain distribution information for CFS hybrid beams, enabling analysis of loads or moments acting on these beams. Tcfs1 and Tcfs2 represent the resultant tensile forces in CFS, Ts1 represents the resultant tensile force in reinforcing steel, and Cc represents the resultant compressive force in the concrete.
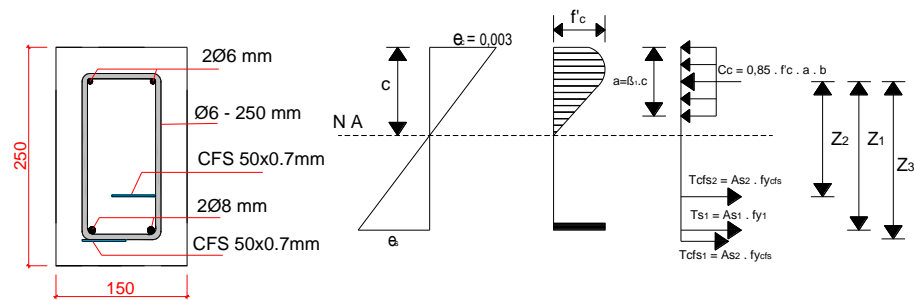
Fig. 1. Stress-strain distribution in CFS hybrid beams

2 Research Methods

The stages of research that have been carried out are as follows:
a. An initial analysis was conducted to determine the dimensions of the beam and the quantity of reinforcement. The primary consideration in determining the dimensions was the maximum load limitation imposed by the laboratory equipment. Additionally, the analysis took into account the theory of the a/d ratio and flexural failure mechanisms. The

preliminary analysis had a beam dimension of 150 x 250 x 1300 mm with 2Ø8 mm bars used as tensile reinforcement and 2Ø6 mm bars as compression reinforcement with stirrups bars Ø6-250 mm as shear reinforcement. The reinforcement details and beam cross-section can be observed in Figure 2.
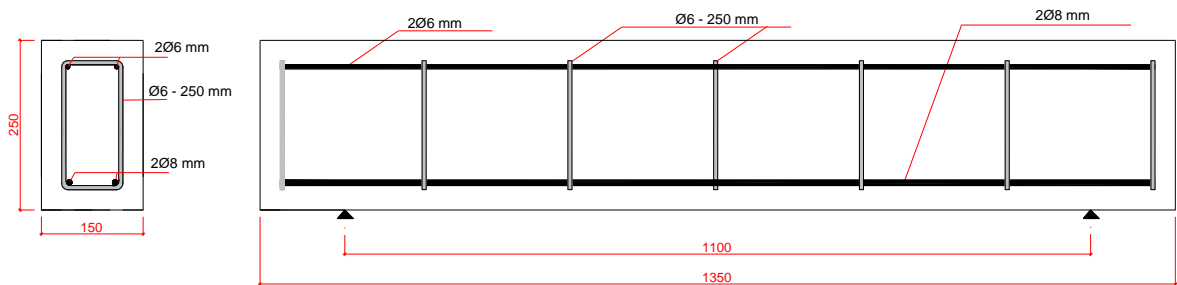
Fig. 2. Cross-section control beam (FB-C)

b. Testing was carried out to determine the material properties of the components comprising the reinforced concrete beam. The testing encompassed coarse and fine aggregate properties, the tensile strength of the reinforcing bar and CFS, as well as the specific gravity of the cement.

c. The mix design was formulated in accordance with the Indonesian National Standard (SNI) 03-2834-2000, targeting a planned concrete strength of 22.5 MPa.

d. A total of 4 test specimens were fabricated, with two specimens serving as control beams (FB-C), and the other two beams incorporating CFS as flexural reinforcement (FB-CFS-1 and FB-CFS-2). In FB-CFS-1, CFS was utilized as square plate reinforcement measuring 50x0.7 mm. In FB-CFS-2, CFS was employed as U-shaped reinforcement with a web width of 32 mm and flange width of 4 mm. The details of the test specimens are depicted in Figures 3 and 4. Figure 2 illustrates the reinforcement layout for FB-C, Figure 3 depicts the reinforcement configuration for FB-CFS-2, and Figure 4 showcases an assembled reinforcement of FB-CFS-1. A spacing of 50 mm between CFS members within the beams was chosen to ensure proper concrete filling between the gaps during the casting process. To determine the actual concrete quality, cylindrical specimens with dimensions of 150 x 300 mm were also created. The CFS tensile reinforcement was crafted into square sections measuring 50 mm by 0.7 mm thick, and with a length of 1300 mm, achieved by cutting and reshaping a C-profile cold-formed steel. This reshaped CFS formed a rectangular shape with dimensions of 90 mm x 190 mm, as illustrated in the following Figure 4.

Fig. 3. Detail U-section CFS flexural beam (FB-CFS-2)

Fig. 4. Detail rectangular shape CFS flexural beam (FB-CFS-1)

e. Flexural testing was conducted by applying a three-point load to the beams. The clear span of the beam was 600 mm, with a distance of 300 mm from the support to the point of loading. Loading was performed using a Hydraulic jack equipped with load indicators on a pressure gauge. Loading was carried out gradually with increments of 2 kN. The test was conducted in accordance with the planned loads derived from the initial analysis, continuing until the beam either failed. The equipment setup and loading process for the beam specimens are illustrated in Figure 5. The data to be recorded during the testing includes the deflection that occurs including deflection at the first crack
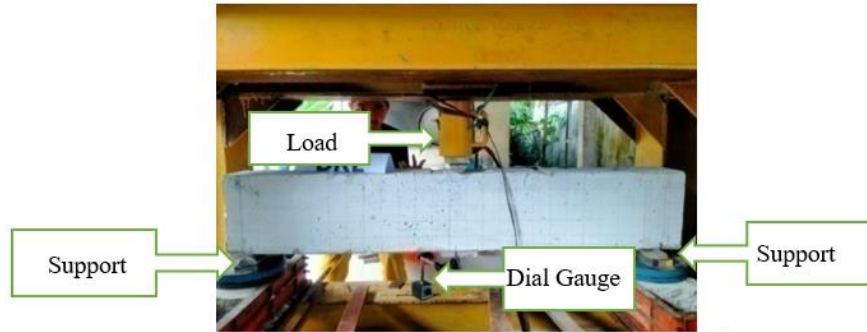
Fig. 5. Flexural loading set-up

3 Results and Discussion

3.1 Material properties

The results of testing coarse aggregate, fine aggregate, and cement properties can be seen in the following Table 1. The average concrete strength obtained from 5-cylinder specimens was 23.145 MPa. The results of tensile testing for bars, as well as 0.7 mm thick CFS, are presented in Table 2.

Table 1. Properties material testing result

	Type of test	Result
Fine aggregate	Zone	III
	Water content (%)	3.17
	Mud content (%)	1.53
	Bulk specific gravity on SSD Basic	2.63
	Water absorption (%)	0.34
	Fineness modulus	3.43
	Grading (mm)	Max. 40
Coarse Aggregate	Water content (%)	3.72
	Mud content (%)	0.27
	Bulk specific gravity on SSD Basic	2.58
	Water absorption (%)	0.95
	Fineness modulus	8.3
Cement	Specific gravity	3.15

Table 2. Tensile test of bar and CFS

Sample	Dimension (mm)	Yield strength (MPa)	Ultimate strength (MPa)
Plain bar 6 mm	5.15	435.71	600.57
Plain bar 8 mm	7.55	374.77	531.48
CFS	12.85 x 0.7	522.11	527.60

3.2 Theoretical analysis

The theoretical analysis carried out refers to SNI 2847-2019 [15] and the results are obtained according to Table 3 below.

Table 3. Theoretical analysis of specimens

Observations	Type of specimens			
	FB-C 1	FB-C 2	FB-CFS 1	FB-CFS 2
Ultimate load (kN)	25.06	25.06	48.05	49.48
Moment (kNm)	6.89	6.89	13.21	13.45

From Table 3, it is evident that the addition of cold-formed steel as tensile reinforcement can theoretically enhance the flexural capacity of the beams. For the improvement of flexural capacity, FB-CFS 1 and FB-CFS 2 are respectively targeted to increase by 91.7% and 97.4%. This difference arises due to the fact that the cross-sectional area of the U-shaped CFS reinforcement in FB-CFS-2 is 4% larger than the flat plate-shaped in FB-CFS-1.

3.3 Flexural specimens testing

The results of flexural strength testing for the control beam (FB-C) and the FB-CFS beam can be observed in Table 4. The relationship between load and deflection for these four specimens is depicted in Figure 6.

In Figure 6, it is evident that the behavior of the control beam and the hybrid beams is significantly different. For the control beam (FB-C-1 and FB-C-2), as it progresses into the cracking stage or when the load exceeds 8 kN, the increase in cracks and capacity becomes nonlinear. At this point, it can be categorized that the beam has entered a nonlinear or inelastic state. With further incremental load, the increase in cracks becomes larger, potentially exceeding the required crack width.

In both flexural hybrid beams, FB-CFS 1 and FB-CFS 2, the load-deflection curve can be divided into two stages: the cracking development stage and the post-failure stage. When reaching the maximum load, the beams still experience increased cracking alongside a decrease in capacity until failure occurs. The deflection observed in the FB-CFS beams is smaller compared to the FB-C beams.

Table 4. Experimental result of specimens

Specimens	Load (kN)		Moment (kNm)	Deflection* (mm)
	First Crack	Maximum		
FB-C 1	7.82	21.49	5.91	22.8
FB-C 2	10.43	23.73	6.53	36.07
FB-CFS 1	12.83	31.52	8.67	7.98
FB-CFS 2	10.17	36.88	10.14	6.93

*at maximum load
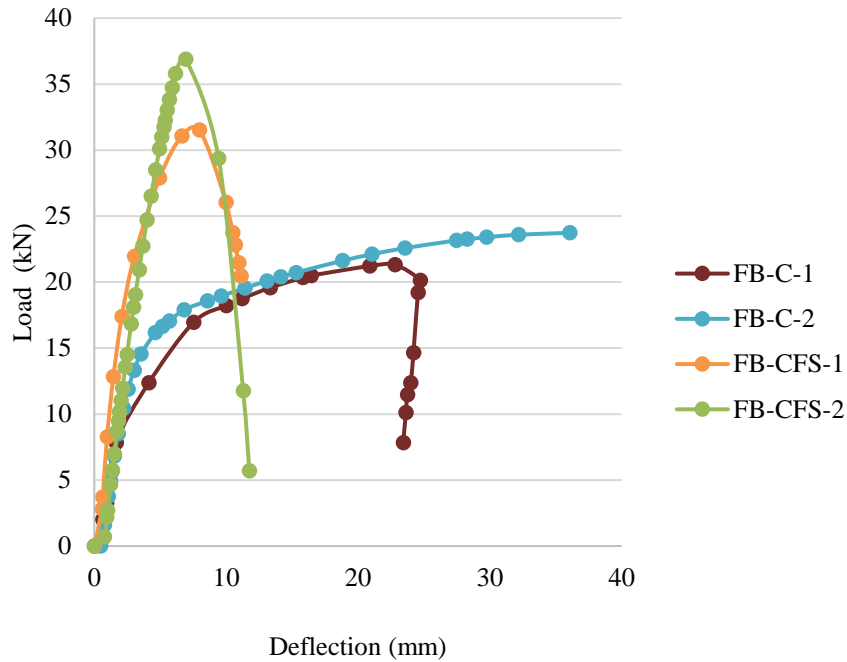
Fig.6. Load versus deflection

When comparing the control beam with the hybrid beam, it's observed that the hybrid beam has a greater load-carrying capacity than the control beam while exhibiting a more brittle behavior than the control beam. This indicates that the addition of CFS as supplementary flexural reinforcement can indeed increase the beam's capacity.

From Table 4, it's also evident that the increase in flexural load capacity for FB-CFS-1 and FB-CFS-2 is 46.65% and 55.43% respectively, compared to the control beam (FB-C-1 and FB-C-2). Additionally, the maximum load in FB-CFS-2 is greater by 17% when compared to the maximum load in FB-CFS-1. This demonstrates that there's an enhancement in the maximum load as the area of CFS reinforcement increases. [9] also mentioned that the C-profile (with a higher reinforcement ratio) used as flexural reinforcement in concrete beams exhibits higher flexural capacity compared to other forms of CFS.

Apart from the increase in flexural capacity, the deflection observed in FB-CFS is significantly smaller compared to the deflection in FB-C. This indicates that FB-CFS beams are stiffer when compared to FB-C beams.

3.4 Stiffness

The assessment of stiffness in the beam is divided into two segments: initial stiffness, which is the stiffness obtained from the beginning of loading until the occurrence of the first crack (crack stiffness), and the second is the stiffness obtained from the maximum load. The calculated stiffness results can be found in Table 5.

Table 5. Beams stiffness

Specimens	Deflection (mm)		Stiffness (N/mm)	
	First Crack	Ultimate	First Crack	Ultimate
FB-C 1	1.65	22.8	4739.52	942.73
FB-C 2	2.21	36.07	4722.49	657.95
FB-CFS 1	1.15	7.98	11160.00	3950.10
FB-CFS 2	1.91	6.93	5329.79	5322.90

The stiffness values of FB-CFS and FB-C beams indicate significant differences in initial stiffness. The initial stiffness of FB-CFS-1 is 1.35 times greater than that of FB-C-1, and the initial stiffness of FB-CFS-2 increases by 12.8% compared to FB-C-2. This indicates that an increase in stiffness occurs before the emergence of the first crack. FB-CFS-1's initial stiffness is twice that of FB-CFS-2, demonstrating that FB-CFS-1 is stiffer than FB-CFS-2 before the occurrence of the initial crack. However, the situation is reversed for the secondary stiffness, with FB-CFS-1 being smaller than FB-CFS-2.

The ultimate stiffness observed in FB-CFS 1 and FB-CFS 2 beams showcases sequential increases of 3.1 times and 7.1 times respectively when compared to FB-C 1 and FB-C 2. This demonstrates that the addition of CFS as tensile reinforcement can enhance the stiffness of the beams, particularly for U-shaped CFS sections. This statement is in line with [16], who stated that using cold-formed steel (CFS) as a replacement for reinforcement in lightweight concrete beams increases the stiffness (MOE) of the beams, ultimate load capacity, and modulus of rupture (MOR).

3.5 Comparison of experimental results to theoretical results

Table 6 displays the results of the comparison between the experimental moment (Mu) and theoretical moment (Mt), as well as the experimental shear force (Vu) and theoretical shear force (Vt). It is evident here that the ratio of the maximum load and moment in FB-CFS is smaller compared to FB-C, indicating that the experimental results for FB-CFS do not yet align with the theoretical analysis.

Table 6. Theoretical and experimental results

Specimens	Moment (kNm) and Load (kN)				Ratio	
	Mu	*Mt*	*Pu*	*Pt*	*Mu/Mt*	*Pu/Pt*
FB-C-1	5.91	6.89	21.49	25.06	0.86	0.86
FB-C-2	6.53	6.89	23.73	25.06	0.95	0.95
FB-CFS-1	8.67	13.21	31.52	48.05	0.66	0.66
FB-CFS-2	10.14	13.45	36.89	49.48	0.75	0.75

Referring to the discussion of Table 3, theoretically, FB-CFS is expected to experience an increase in flexural capacity of around 91-97%. However, experimental results show that FB-

CFS only exhibits a flexural capacity increase of approximately 46-55%. This discrepancy might be attributed to the occurrence of slip in the CFS due to inadequate bonds between the CFS and the concrete. Additionally, the surface of the CFS, being coated with Zinc-Alloy, contributes to its smoothness. [17] mentioned that CFS when integrated with concrete would be more effective if measures such as adding shear connectors, such as bolts, or modifying the cross-section to address slip between the CFS and concrete were implemented.

3.6 Crack pattern

The first crack in FB-C-1 occurred at a load of 7.8 kN, where the crack developed in the middle of the beam's bottom surface, extending towards the direction of the load. This initial crack spanned nearly 15 cm from the bottom of the beam. As the load increased, the crack progressively lengthened along the load direction. Upon reaching the maximum load of 21.49 kN, the crack width at the mid-span area widened significantly, and the tensile reinforcement ultimately fractured. The failure mode observed in FB-C is a pure flexural failure, as depicted in Figure 7.

Fig.7 FB-C-1 crack pattern

Fig.8 FB-CFS-1 crack pattern

In contrast to the control beam, the initial crack in FB-CFS-1 appeared at a load of 12.83 kN, originating precisely at the midpoint of the lower surface of the beam and propagating toward the direction of the applied load. As the load increased, diagonal cracks emerged on the lower section of the beam, extending towards the load point. Upon reaching the ultimate load of 31.52 kN, the crack width at the mid-span region significantly widened, causing disruption within the tensile component. The mode of failure observed in FB-CFS-1, depicted in Figure 8, is also classified as a flexural failure.

4 Conclusion

Drawing from the conducted research, it can be deduced that:
The inclusion of CFS as tensile reinforcement can enhance the beam's capacity by 46.65% and 55.43% compared to the control beam. Sequential increases in stiffness of 3.1 times and 7.1 times greater were observed when compared to FB-C 1 and FB-C 2, respectively. Overall, the failure mode observed is a flexural failure.

Acknowledgements

References

[1] H. Shirato, Garam Air Laut Pengaruhi Kekuatan Beton dan Konstruksi, Unika.Ac.Id. (2015). https://www.unika.ac.id/news/media-massa/online/garam-air-laut-pengaruhi-kekuatan-beton-dan-konstruksi/ (accessed September 5, 2022).

[2] Elviana, A. Saputra, D. Sulistyo, The Influence of Sea Water Content on the Shear Strength of Reinforced Concrete Beams, J. Phys. Conf. Ser. 1625 (2020). https://doi.org/10.1088/1742-6596/1625/1/012027.

[3] F. Yuan, M. Chen, Numerical sensing of plastic hinge regions in concrete beams with hybrid (FRP and steel) bars, Sensors (Switzerland). 18 (2018). https://doi.org/10.3390/s18103255.

[4] P.V.V. GangaRao, Hota VS, Narendra Taly, Reinforced Concrete Design with FRP Composites, CRC Press. Taylor Fr. Gr. Boca Raton, FL, USA. (n.d.). https://books.google.co.id.

[5] P.V.V. and H.V.S. GangaRao, Bending Behavior and Deformability of Glass Fiber-Reinforced Polymer Reinforced Concrete Members, ACI Struct. J. 98 (2001). https://doi.org/10.14359/10750.

[6] Y. Tang, Z. Wu, Distributed long-gauge optical fiber sensors based self-sensing FRP bar for concrete structure, Sensors (Switzerland). 16 (2016). https://doi.org/10.3390/s16030286.

[7] H.T. Wang, G. Wu, Y.Y. Pang, Theoretical and numerical study on stress intensity factors for FRP-strengthened steel plates with double-edged cracks, Sensors (Switzerland). 18 (2018). https://doi.org/10.3390/s18072356.

[8] R.A. Hawileh, M.Z. Naser, Thermal-stress analysis of RC beams reinforced with GFRP bars, Compos. Part B Eng. 43 (2012) 2135–2142. https://doi.org/https://doi.org/10.1016/j.compositesb.2012.03.004.

[9] C.C.S. Khala, Basyaruddin, M.S. Muslimin, A.P. Putri, Uji Lentur Balok Beton Bertulang Baja Ringan Dengan Skema Tulangan Tunggal, Teras J. 11 (2021) 171. https://doi.org/10.29103/tj.v11i1.418.

[10] K. Alenezi, T. Alhajri, M.M. Tahir, M.R.K. Badr, S.O. Bamaga, Strengthen of Cold-Formed Steel Column with Ferrocement Jacket : Push out Tests, 7 (2013) 63–66.

[11] E. Taheri, A. Firouzianhaji, P. Mehrabi, B.V. Hosseini, B. Samali,

Experimental and numerical investigation of a method for strengthening cold-formed steel profiles in bending, Appl. Sci. 10 (2020). https://doi.org/10.3390/app10113855.

[12]	A. Kadir, I. Satyarno, A. Awaludin, J. Teknik, F. Teknik, U.G. Mada, J. Teknik, F. Teknik, U.G. Mada, D.I. Yogyakarta, Kekuatan Lateral Dinding Cold-Formed Steel Strap Braced Pada Rumah Instan Sehat Baja Ringan (Risbari), (2021) 136–143.

[13]	I. Puluhulawa, A. Alamsyah, R. Husna, The Behavior of Reinforced Concrete Beams Added Cold-Formed-Steel as Shear Reinforcement, J. Struct. Monit. Built Environ. 2 (2022) 8–15. https://doi.org/10.30880/jsmbe.2022.02.01.002.

[14]	I. Puluhulawa, Alamsyah, Behavior of Shear Connector Variations on Strengthened Reinforced Concrete Slabs Using Cold Formed Steel, IOP Conf. Ser. Earth Environ. Sci. 498 (2020) 1–7. https://doi.org/10.1088/1755-1315/498/1/012050.

[15]	Badan Standardisasi Nasional, Persyaratan Beton Struktural untuk Bangunan Gedung, Sni 2847-2019. (2019) 720.

[16]	Mahmuda, Revias, S. Indra, Sumiati, The Use of Cold-Formed Steel as a Substitute for Reinforcement on Structural of Lightweight Concrete Beams, Proc. 4th Forum Res. Sci. Technol. 7 (2021) 294–299. https://doi.org/10.2991/ahe.k.210205.050.

[17]	J. M.Irwan, A.H. Hanizah, I. Azmi, Test of shear transfer enhancement in symmetric cold-formed steel-concrete composite beams, J. Constr. Steel Res. 65 (2009) 2087–2098. https://doi.org/10.1016/j.jcsr.2009.07.008.